10458 *Biochemistry* **2010,** *49,* 10458–10472
DOI: 10.1021/bi101577p

BIOCHEMISTRY
including biophysical chemistry & molecular biology
Article

Insights into Nucleotide Recognition by Cell Division Protein FtsZ from a *mant*-GTP Competition Assay and Molecular Dynamics†

Claudia Schaffner-Barbero,‡ Rubén Gil-Redondo,§ Laura B. Ruiz-Avila,‡ Sonia Huecas,‡ Tilman Läppchen,∥,⊥ Tanneke den Blaauwen,∥ J. Fernando Diaz,‡ Antonio Morreale,§ and Jose M. Andreu*,‡

‡*Centro de Investigaciones Biológicas, CSIC, Ramiro de Maeztu 9, 28040 Madrid, Spain,* §*Bioinformatics Unit, Centro de Biología Molecular Severo Ochoa, UAM-CSIC, Nicolás Cabrera 1, 28049 Madrid, Spain, and* ∥*Swammerdam Institute for Life Sciences, Molecular Cytology, Science Park 904, 1098 XH Amsterdam, The Netherlands.* ⊥*Present address: Department of Biomolecular Engineering, Philips Research, High Tech Campus 11, M/S WBC02 P263, 5656 AE Eindhoven, The Netherlands*

Received September 29, 2010; Revised Manuscript Received November 3, 2010

ABSTRACT: Essential cell division protein FtsZ forms the bacterial cytokinetic ring and is a target for new antibiotics. FtsZ monomers bind GTP and assemble into filaments. Hydrolysis to GDP at the association interface between monomers leads to filament disassembly. We have developed a homogeneous competition assay, employing the fluorescence anisotropy change of *mant*-GTP upon binding to nucleotide-free FtsZ, which detects compounds binding to the nucleotide site in FtsZ monomers and measures their affinities within the millimolar to 10 nM range. We have employed this method to determine the apparent contributions of the guanine, ribose, and the α-, *β*-, and *γ*-phosphates to the free energy change of nucleotide binding. Similar relative contributions have also been estimated through molecular dynamics and binding free energy calculations, employing the crystal structures of FtsZ−nucleotide complexes. We find an energetically dominant contribution of the *β*-phosphate, comparable to the whole guanosine moiety. GTP and GDP bind with similar observed affinity to FtsZ monomers. Loss of the regulatory *γ*-phosphate results in a predicted accommodation of GDP which has not been observed in the crystal structures. The binding affinities of a series of C8-substituted GTP analogues, known to inhibit FtsZ but not eukaryotic tubulin assembly, correlate with their inhibitory capacity on FtsZ polymerization. Our methods permit testing of FtsZ inhibitors targeting its nucleotide site, as well as compounds from virtual screening of large synthetic libraries. Our results give insight into the FtsZ−nucleotide interactions, which could be useful in the rational design of new inhibitors, especially GTP phosphate mimetics.

FtsZ is a cytoskeletal protein essential for bacterial cell division that forms the Z-ring at the midcell and is anchored to the membrane by FtsA and ZipA (*1*−*4*). FtsZ with an added membrane tag can constrict liposomes in the absence of other cellular components (*5*). FtsZ and its eukaryotic homologue tubulin share the same fold despite low sequence similarity (*6*, *7*). Both are self-assembling cytoskeletal GTPases with an N-terminal nucleotide binding domain and a GTPase activating domain. These similarities lend weight to the idea that FtsZ and tubulin share a common ancestor (*8*). Despite their structural homology, FtsZ and tubulin present different functions and assembly dynamics. FtsZ forms similar protofilaments to tubulin (*9*, *10*) but does not form microtubules.

FtsZ assembly is dependent on nucleotide binding and hydrolysis, where GTP favors assembly and GDP favors disassembly. The nucleotide binding site is located at the top end of the FtsZ monomer, with the complete GTPase site formed by the N-domain of one monomer and the C-domain of the next monomer in the protofilament (*10*, *11*). Unlike in tubulin, where the nucleotide site is completely occluded in the assembled protofilament (*7*), assembled FtsZ presents an exposed nucleotide binding site capable of nucleotide exchange in the polymerized state. However, the dissociation rate for nucleotide in polymerized FtsZ is probably slow enough to allow FtsZ monomers to recycle with GTP hydrolysis in a similar manner to tubulin (*12*, *13*). Assembly is cooperative despite the single-stranded nature of FtsZ protofilaments. Several models have been proposed to explain this behavior through an initial monomer isomerization step (*14*−*16*). A combined computational and mutational analysis suggests that a simultaneous contact of a GTP-bound subunit with adjacent top and bottom subunits forces a conformational change involving a closure rotation of core helix H7 onto the C-terminal domain. This assembly switch may govern the acquisition of the straight form and the activation of GTPase activity (*17*).

The near universality of FtsZ in bacteria makes it an attractive target for the development of novel antibiotics that could combat the emergence of pathogenic bacterial strains resistant to current therapeutic options (*18*, *19*). Several compounds have been reported

†We wish to dedicate this paper to the memory of our colleague Ángel R. Ortiz, who passed away May 5, 2008, at the age of 41 and with whom this work was started. This work was supported by grants from the Spanish Ministry for Science (MCINN) BFU2008-00013 (J.M.A.), Madrid Community S-BIO-0214-2006 (A.M. and J.M.A.), and "Vernieuwingsimpuls" Grant 016.001.024, (T.d.B.) of The Netherlands Organization for Scientific Research (NWO). C.S.-B. and L.B.R.-A. had FPI predoctoral fellowships. R.G.-R. had a contract from MCINN "Programa de Personal Técnico y de Apoyo 2008". We thank OpenEye Scientific Software, Inc., for providing us with academic license for their software. Barcelona Supercomputing Center is acknowledged for the generous allocation of computer time.

*Corresponding author: phone, 34 91 8373112; fax, 91 5360432; e-mail, j.m.andreu@cib.csic.es.

 Published on Web 11/08/2010

to inhibit FtsZ activity, including zantrins, sanguinarine, cinnamaldehyde, and totarol (*20*−*23*) among others (see a list in Supporting Information Table S1). One compound in particular, PC190723, is an effective protector against lethal doses of *Staphylococcus aureus* in a mouse model of infection, which has validated FtsZ as a target for antibacterial intervention. It appears to bind in the channel between the N- and C-terminal domains of FtsZ that overlaps the taxol binding site in tubulin (*24*). This, coupled to its ability to prevent FtsZ polymer disassembly, makes PC190723 a candidate to constitute the founding member of a new class of FtsZ polymer stabilizing agents (*25*).

In addition to these compounds, a series of GTP analogues with C8 substitutions have the capacity to specifically inhibit purified FtsZ while supporting the assembly of eukaryotic tubulin. This revealed differences between the GTP binding sites of both proteins (*26*, *27*). It points to the interfacial FtsZ nucleotide binding site as a potential target for the development of new antibacterial agents (*28*). Despite the attractive nature of the FtsZ nucleotide binding site as a target, the precise characteristics of the interaction of FtsZ with GTP and GDP are not yet fully resolved. In addition, the search for inhibitors that could specifically target the FtsZ nucleotide site would greatly benefit from a robust and precise method for characterizing molecules that could substitute the nucleotide.

In this study we have developed and validated a competition method employing nucleotide-free FtsZ (apoFtsZ) monomers and the fluorescent nucleotide *mant*-GTP,[1] which allows the efficient characterization of compounds that specifically target the GTP binding site of FtsZ. We have investigated how the different parts of the GTP molecule contribute to the binding to FtsZ employing this assay, molecular dynamics, and free energy calculations. Our method has allowed more precise measurements of the binding affinities of the C8-substituted GTP analogues, which correlated with their inhibitory capacity on FtsZ from two different bacterial species. Finally, we have exemplified the use of our method with a selection of previously reported FtsZ inhibitors and molecules from virtual screening, testing them for binding to the nucleotide site.

EXPERIMENTAL PROCEDURES

Small Molecules. *mant*-GTP, *mant*-GDP, and 8-Br-GTP (BrGTP) were from Jena Bioscience. GTP, GDP, GMP, guanosine, ATP, CTP, UTP, cinnamaldehyde, sanguinarine, and acetate kinase (from *Escherichia coli*) were from Sigma. Acetyl phosphate (lithium potassium salt) was from Fluka. Totarol was a gift from Mende Biotech. [8-^{3}H]GTP (5.1 Ci/mmol) was from Amersham Biosciences. Potassium phosphate (inorganic phosphate, P_i) was from Merck, potassium pyrophosphate (PP_i) was from Riedel de Haën, and sodium triphosphate (PPP_i) was from Fluka. 8-Methoxy-GTP (MeOGTP), 8-pyrrolidino-GTP (PyrrGTP), 8-morpholino-GTP (MorphGTP), 8-Cl-GTP (ClGTP), 8-I-GTP (IGTP), and 8-*tert*-butyl-GTP (*t*BuGTP) were prepared as reported (*26*, *27*). Their stock solutions were made in 25 mM Pipes−KOH, 50 mM KCl, 1 mM EDTA, and 10 mM $MgCl_2$, pH 7.5. Compounds selected by virtual screening (see below) were purchased from ChemBridge and IBScreen and dissolved in spectroscopy grade dimethyl sulfoxide. Their absorption spectra were acquired, and their potential interference with *mant*-GTP fluorescence measurements was characterized. Their practical solubility in buffer containing 2% residual dimethyl sulfoxide was determined spectrophotometrically after centrifugation at 89000*g* (50000 rpm) for 15 min in a TLA120.2 rotor at 25 °C with a Beckman TLX ultracentrifuge.

Molecular Dynamics, Structural Analysis, and Binding Free Energy Calculations. The initial model structures for FtsZ from the thermophilic archaea *Methanococcus jannaschii* complexed with GTP-magnesium or GDP were taken from the Protein Data Bank entries 1W5A (chain A, named 1W5A-A) and 2VAP, respectively. The positions of hydrogen atoms were assigned with the H++ web server (*29*). The Poisson−Boltzmann (PB) method (*30*) was used, at pH 7.4, 0.15 M salt concentration, with internal and external dielectric constants of 4 and 80, respectively. Based on the information provided by H++, the following residues were protonated: H183, H288, and E293 in 2VAP and H288 in 1W5A. Standard atomic charges and radii were assigned according to the ff99 force field (*31*). The two models were immersed in cubic boxes of TIP3P water molecules (*32*) large enough to guarantee that the shortest distance between the solute and the edge of the box was greater than 15 Å. Counterions were also added to maintain electroneutrality. Three consecutive minimizations were performed: (i) involving only hydrogen atoms, (ii) involving only the water molecules and ions, and (iii) involving the entire system. The starting structures, prepared as indicated above, were simulated in the NPT (*N*, total number of atoms; *P*, pressure; *T*, temperature) ensemble with the periodic boundary conditions and particle mesh Ewald method to treat long-range electrostatic interactions. The systems were then heated and equilibrated in two steps: (i) 20 ps of MD heating the whole system from 100 to 300 K and (ii) equilibration of the entire system during 100 ps at 300 K. The equilibrated structures, with rmsd to the crystal structures of 0.4−0.5 Å, were the starting points for 50 ns MD simulations at constant temperature (300 K) and pressure (1 atm). The constraint algorithm SHAKE was used to keep bonds involving H atoms at their equilibrium length, allowing a 2 fs time step for the integration of Newton's equations of motion. The ff99 and TIP3P force fields were used to describe the proteins and water molecules, respectively, as implemented in the AMBER 10 package (*33*). The entire trajectories, the last part (last 0.5 ns) of each 10 ns fraction, and the last part (last 0.5 ns) of the whole trajectories were used to sample frames at 10 ps intervals, which were subsequently used for structural and energetic analysis.

Average structures, mass-weighted rmsds, with and without fitting to the minimized X-ray structures (taken as reference), and configuration entropies (see below) were calculated with the ptraj program included in the AMBER 10 package. The averaged structures were minimized in vacuum with the ff99 force field, without periodic boundary conditions and during 1000 steps (the first 500 with the steepest descent method and the rest with the conjugated gradient) solely to alleviate the possible clashes that may be originated by averaging the coordinates.

Hydrogen bonds were calculated with HBonds Plugin (version 1.1) as implemented in the molecular visualization program VMD (*34*). A hydrogen bond is formed when both the donor−acceptor distance is less than 3.0 Å and the donor−hydrogen−acceptor angle is less than 20°. The hydrogen bond occupancy parameter is defined as ratio of times where the hydrogen bond is present relative to the total time length of the trajectory.

[1]Abbreviations: *mant*-GTP, 2/3-*O*-(*N*-methylanthraniloyl)guanosine 5′-triphosphate; *mant*-GDP, 2/3-*O*-(*N*-methylanthraniloyl)guanosine 5′-diphosphate; MeOGTP, 8-methoxyguanosine 5′-triphosphate; PyrrGTP, 8-pyrrolidinoguanosine 5′-triphosphate; ClGTP, 8-chloroguanosine 5′-triphosphate; BrGTP, 8-bromoguanosine 5′-triphosphate; IGTP, 8-iodoguanosine 5′-triphosphate; *t*BuGTP, 8-*tert*-butylguanosine 5′-triphosphate; MorphGTP, 8-morpholinoguanosine 5′-triphosphate; Pipes, 1,4-piperazinediethanesulfonic acid; MD, molecular dynamics; MM-GBSA, molecular mechanics-generalized Born model-surface area; rmsd, root-mean-square deviation; VS, virtual screening.

Effective binding free energies (enthalpic contribution) were estimated using the MM-GBSA approach (*35*). The MM-GBSA method approaches free energy of binding as a sum of a molecular mechanics (MM) interaction term, a solvation contribution through a generalized Born (GB) model, and a surface area (SA) contribution to account for the nonpolar part of desolvation. These calculations were performed for each sampled snapshot (see above) from the simulations using the appropriate module within the AMBER 10 package and averaged out. The total values were partitioned into individual residue contributions to allow for a finer analysis. The individual interactions were assigned to the different parts of the GDP and GTP molecules (guanine and ribose rings, α-, *β*-, and *γ*-phosphate groups) based on visual inspection (empirical formulas that can be found in the Supporting Information section). Configurational entropies were also calculated with the ptraj program. Briefly, the mass-weighted covariance matrix was obtained from the dynamics simulations and diagonalized. The eigenvalues were then converted into frequencies after quasi-harmonic analysis (*36*, *37*). Finally, standard statistical mechanics formulas were used to obtain the entropy values.

Virtual Screening (*VS*). All VS calculations have been performed using the VSDMIP platform (*38*) following a common protocol (*39*) comprised of filtering with DOCK (*40*), docking with CDOCK (*41*), and rescoring with AMBER 10 (*33*) and MM-GBSA energy analysis (*35*). Briefly, FtsZ chain A from the crystal structure of SulA:FtsZ (PDB ID 1OFU) from the pathogen *Pseudomonas aeruginosa* was used as receptor after removing the nucleotide, water molecules, and ions. The AMBER 10 ff99 force field (*33*) was then used to assign atom types and atomic charges for each atom. Hydrogen atoms were added assuming standard protonation states of titratable groups. The ChemBridge and IBScreen chemical libraries, containing 454886 and 355138 compounds, respectively, most of them drug-like molecules fullfiling Lipinski's rules (*42*), were directly obtained from ZINC 6 (*43*) in SMILES format and prepared with VSDMIP (*38*). The binding site was built around the position of the deleted nucleotide adding a 5.0 Å cushion to its maximum dimensions for the filter step and 7.5 Å for the docking step. Binding site hot spots (represented by spheres) used by DOCK were generated by GAGA (*44*). After docking the molecules with DOCK and applying a ZScore cutoff value of 4.5 on the contact scores obtained, 2055 molecules were selected for the next step in the case of ChemBridge database. The IBScreen library was screened without employing the DOCK filter. These molecules were then further screened with CDOCK employing a grid spacing of 0.5 Å and the best 100 classified passed to the rescoring step. Rescoring was performed to take into account full flexibility and explicit solvent effects via molecular dynamics simulations and postprocessing the trajectories with MM-GBSA method to estimate the free energy of binding. Both steps were performed as stated before except that the length of the trajectories was set to 1 ns and the MM-GBSA analysis restricted to the last 200 ps. Search for analogous compounds, when needed, was performed through the ZINC server utilities and then submitted to the docking and rescoring steps as explained above.

ApoFtsZ Preparation and Evaluation. Stable apoFtsZ from *M. jannaschii* was prepared and its concentration measured spectrophotometrically as described (*12*, *45*). *M. jannaschii* FtsZ was chosen due to its capacity to retain structure and functionality after nucleotide removal, unlike bacterial FtsZ from *E. coli* (*45*). ApoFtsZ functionality was checked by monitoring its assembly with 90° light scattering at 350 nm, employing a Horiba-Jobin-Yvon FluoroMax-4 spectrofluorometer. ApoFtsZ was diluted to 12.5 μM in 25 mM Pipes−KOH, 50 mM KCl, and 1 mM EDTA, pH 7.5 at 55 °C. Polymerization was induced by addition first of 10 mM $MgCl_2$ and then of 1 mM GTP. All further assays employing apo-FtsZ were done in the same buffer with 10 mM $MgCl_2$ at 25 °C. The nucleotide binding capacity of apoFtsZ was determined as described (*12*) with modifications. Briefly, samples were prepared at varying concentrations of *mant*-GTP (3−15 μM) with or without apoFtsZ (5 μM) and then centrifuged at 355000*g* (100000 rpm) for 2.5 h in a TLA 120.2 rotor at 25 °C. *mant*-GTP concentrations were determined from their absorption spectra in the protein-depleted top half of the tubes employing an extinction coefficient $\varepsilon_{254} = 23300\ M^{-1}\ cm^{-1}$ (*12*). Bound *mant*-GTP was determined from the difference of *mant*-GTP concentration between samples containing apoFtsZ or not. The resulting number of *mant*-GTP binding sites (*n*) was 0.75 ± 0.04, compatible with the previously reported *mant*-GTP stoichiometry 0.83 ± 0.08 employing the same method (*12*) and with subsequent results. The difference to unity may be due to a fraction of inactive protein. In all cases apoFtsZ concentration refers to concentration of nucleotide binding sites, except where explicitly stated.

FtsZ Polymerization Assays. FtsZ from *E. coli* and *Bacillus subtilis* was expressed and purified as described (*25*). Samples (50 μL) were prepared in polycarbonate ultracentrifuge tubes in a thermostat at 37 °C (for FtsZ from *E. coli*) or 25 °C (for FtsZ from *B. subtilis*) with varying concentrations of GTP analogues. FtsZ from *E. coli* was diluted to 9 μM in 50 mM Hepes−NaOH, 50 mM KCl, and 10 mM $MgCl_2$, pH 7.5 (*26*, *27*), with a GTP regenerating system consisting of 15 mM acetyl phosphate and 1 unit/mL acetyl kinase. Samples were incubated for 10 min; polymerization was induced by addition of 60 μM GTP, and samples were centrifuged at 386000*g* (100000 rpm) for 10 min at 37 °C in a TLA-100 rotor (Beckman). Samples of 9 μM FtsZ from *B. subtilis* were prepared in 50 mM Mes−KOH, 50 mM KCl, 1 mM EDTA, and 10 mM $MgCl_2$, pH 6.5 (*25*), also employing the GTP regenerating system, polymerization was initiated by addition of 60 μM GTP, and samples were centrifuged for 20 min at 25 °C as above. Control samples included one with 1 mM GDP (without GTP and regenerating system) and another with no nucleotide. Supernatants were removed, and 1 equivalent volume of SDS sample buffer was added to them. Pellets were resuspended in 1 volume of sample buffer plus 1 volume of buffer (FtsZ from *B. sutbtilis*) or in $^1/_3$ volume of buffer and $^1/_3$ volume of sample buffer (FtsZ from *E. coli*). Pellet and supernatant aliquots from each sample were loaded with a 15 min eletrophoretic shift between them into the same lanes of SDS−12% polyacrylamide gels. Gels were stained with Coomassie blue, scanned using a Bio-Rad CS-800 calibrated densitometer, and analyzed with Quantity One software (Bio-Rad).

^{3}H-GTP Binding Measurements. Assays employing ^{3}H-GTP, apoFtsZ, and competing ligands (where applicable) were prepared at the desired concentrations and centrifuged as reported (*12*), and for this work the concentration of free ^{3}H-GTP ($[^3H\text{-}GTP]_f$) was determined in the protein-depleted top half of tubes, after dilution in 3.8 mL of Beckman ReadySafe solution, employing a 1219 Rackbeta liquid scintillation counter (LKB Wallac) operating with a 55% efficiency. The ^{3}H-GTP concentration is proportional to the detected activity in counts per minute (cpm). We calculated a factor to correct for the amount of ^{3}H-GTP sedimented in the absence of protein

$$F_s = cpm_{bt\text{-}0}/cpm_{top\text{-}0} \quad (1)$$

where $cpm_{bt\text{-}0}$ and $cpm_{top\text{-}0}$ are the activities in the bottom half and top half of tubes centrifuged in the absence of apoFtsZ.

Controls without apoFtsZ were included in each assay to measure this correction factor, with typical values of 1.4 ± 0.1. The concentration of bound ^{3}H-GTP was calculated as

$$[^3\text{H-GTP}]_b = [(\text{cpm}_T - \text{cpm}_{top}(1+F_s))/\text{cpm}_T][^3\text{H-GTP}]_T \quad (2)$$

where cpm_T and cpm_{top} are the total activity ($\text{cpm}_T = \text{cpm}_{bt\text{-}0} + \text{cpm}_{top\text{-}0}$) and the activity found in the protein-depleted top half of the sample, respectively, and $[^3\text{H-GTP}]_T$ and $[^3\text{H-GTP}]_b$ are the total and bound concentrations of ^{3}H-GTP, respectively. The free ^{3}H-GTP concentration is $[^3\text{H-GTP}]_{free} = F_s[^3\text{H-GTP}]_{top}$. Less than 2% of total ^{3}H-GTP was left in the tubes.

^{3}H-GTP and ApoFtsZ Titrations. ^{3}H-GTP (50 nM, 51 nCi) was titrated with increasing concentrations of apoFtsZ. Bound and free ^{3}H-GTP were determined as explained above. Assuming each ^{3}H-GTP binds one apoFtsZ, the following equations apply:

$$[P]_f = [P]_T - [^3\text{H-GTP}]_b \quad (3)$$

$$[^3\text{H-GTP}]_b/[^3\text{H-GTP}]_T = (K_{^3\text{H-GTP}}[P]_f)/(1+K_{^3\text{H-GTP}}[P]_f) \quad (4)$$

where $[P]_T$ and $[P]_f$ are the total and free concentrations of apoFtsZ binding sites and $K_{^3\text{H-GTP}}$ is the equilibrium binding constant of ^{3}H-GTP to apoFtsZ. Equation 4 was employed to obtain the best-fitted value of $K_{^3\text{H-GTP}}$ with a nonlinear least-squares Marquadt algorithm.

ApoFtsZ (75 nM) was then titrated with increasing concentrations of ^{3}H-GTP. Mixtures of ^{3}H-GTP and GTP were used with activities ranging from 8 nCi to 0.5 μCi per sample. Concentrations of free and bound ^{3}H-GTP were determined and the equation for binding to independent sites

$$[^3\text{H-GTP}]_b/[P]_T = (nK_{^3\text{H-GTP}}[^3\text{H-GTP}])/(1+K_{^3\text{H-GTP}}[^3\text{H-GTP}]) \quad (5)$$

was iteratively applied to fit the $[^3\text{H-GTP}]_b/[P]_T$ vs $[^3\text{H-GTP}]_f$ data to obtain the best-fitted value of n (binding sites of ^{3}H-GTP per total apoFtsZ) and $K_{^3\text{H-GTP}}$.

Ligand Competition with ^{3}H-GTP. Samples containing 75 nM apoFtsZ and 100 nM ^{3}H-GTP were prepared with increasing concentrations of test ligand in Pipes−Mg^{2+} buffer and processed as described above. To measure the binding affinity of a test ligand (L) displacing the reference ligand ^{3}H-GTP from its apoFtsZ binding site, unitary stoichiometry was assumed, the fractional binding of ^{3}H-GTP was determined, and the following expressions were applied

$$K_{^3\text{H-GTP}} = [P\cdot{}^3\text{H-GTP}]/([P]_f[^3\text{H-GTP}]_f) \quad (6)$$

$$K_{(L)} = [P\cdot L]/([P]_f[L]_f) \quad (7)$$

$$[^3\text{H-GTP}]_f = [^3\text{H-GTP}]_T - [P\cdot{}^3\text{H-GTP}] \quad (8)$$

$$[L]_f = [L]_T - [P\cdot L] \quad (9)$$

$$[P]_f = [P]_T - [P\cdot L] - [P\cdot{}^3\text{H-GTP}] \quad (10)$$

where $[P\cdot{}^3\text{H-GTP}]$ is the concentration of bound ^{3}H-GTP and $[L]_T$, $[L\cdot P]$, and $[L]_f$ are the total, bound, and free problem ligand concentrations, respectively. A personal computer program EQUIGRA v5 (*46*), implementing the third degree equation resultant from solving eqs 6−10, was employed to find the best least-squares fit value of the equilibrium binding constant of the competing ligand $K_{(L)}$ to the $[^3\text{H-GTP}]_b/[^3\text{H-GTP}]_T$ versus $[L]_T$ data, using the known values of $[P]_T$, $[L]_T$, $[^3\text{H-GTP}]_T$, and $K_{^3\text{H-GTP}}$.

Fluorescence Binding Measurements. Measurements were acquired using a Horiba-Jobin-Yvon Fluorolog 3-221 spectrofluorometer. Anisotropy (r) measurements were collected with vertically polarized excitation and corrected for the sensitivity of each channel with horizontally polarized excitation using a T-format mode (*47*). Fluorescence and binding measurements were modified from a previous study (*12*). Anisotropy and magic angle (I_M) measurements of *mant*-GTP were acquired using 375 nm excitation with a 5 nm band-pass and 445 nm emission with a 10 nm band-pass. Blank values with no *mant*-GTP were subtracted from the raw measurements.

Titration of mant-Nucleotides and ApoFtsZ. Given the necessity of simultaneously measuring anisotropy values (see below), fluorescence intensity was obtained using "magic angle" settings [vertically polarized light for excitation and a 54.7° angle for emission (*47*)] which effectively gave measurements proportional to nonpolarized light. The fraction bound probe (ν_b) is

$$\nu_b = [mant\text{-GTP}]_b/[mant\text{-GTP}]_T = (I_M - I_{Mf})/(I_{Mb} - I_{Mf}) \quad (11)$$

where $[mant\text{-GTP}]_T$ and $[mant\text{-GTP}]_b$ are the total and bound concentrations of *mant*-GTP, I_M is the measurement of the fluorescence intensity of the sample, I_{Mf} is the intensity of free *mant*-GTP, and I_{Mb} is the intensity of bound *mant*-GTP. Given eq 11, for a one to one binding:

$$I_M = (I_{Mf} + K_{mGTP}[P]_f I_{Mb})/(1+K_{mGTP}[P]_f) \quad (12)$$

where K_{mGTP} is the equilibrium binding constant of *mant*-GTP to apoFtsZ. Equation 12 was iteratively applied to fit the I_M vs $[P]_f$ data, from which the best-fitted values for K_{mGTP}, I_{Mf} (which coincided with the measured value), and I_{Mb} were obtained. An intensity factor to be employed in the anisotropy binding measurements below is defined as

$$R = I_{Mb}/I_{Mf} \quad (13)$$

Binding of *mant*-GTP to apoFtsZ was measured through changes in its anisotropy. The anisotropy of a mixture of free and bound fluorophore can be expressed as

$$r = F_b r_b + F_f r_f \quad (14)$$

where r is the measured anisotropy, F_f and F_b are the fractional fluorescence intensities of free and bound fluorophore, respectively, r_f is the anisotropy of free fluorophore, and r_b is the anisotropy of bound fluorophore. In the simplest case of a fluorescent probe with no quantum yield difference between the bound and free state (*48*), the fraction of bound (ν_b) and free (ν_f) fluorophore coincides with the fluorescence fractions for bound and free fluorophore (F_b and F_f, respectively). Employing eq 14 and knowing that the sum of the fluorescence fractions is by definition 1, we obtain

$$\nu_b = (r - r_f)/(r_b - r_f) \quad (15)$$

However, *mant*-GTP does not exhibit this behavior, because there is a difference between the fluorescence intensity of bound and free *mant*-GTP. In this case the fluorescence fraction is

$$F_b = \nu_b(I_b/I_T) \quad (16)$$

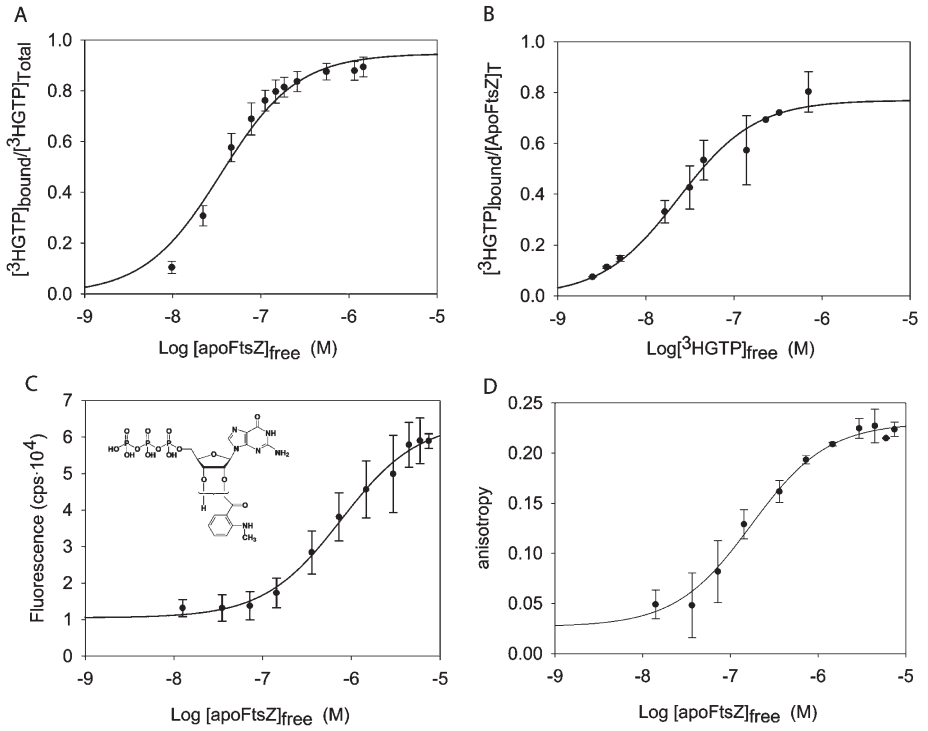

FIGURE 1: Titrations of reference nucleotides and apoFtsZ. (A) Titration of ^{3}H-GTP (50 nM) with apoFtsZ. (B) Titration of apoFtsZ (75 nM) with ^{3}H-GTP. ApoFtsZ concentration in this case refers to total protein concentration to reflect the measurement of binding sites. (C, D) Titration of *mant*-GTP (panel C inset; 50 nM) with apoFtsZ using fluorescence intensity at magic angle and anisotropy, respectively. Data are average and standard deviations from three independent measurements. Lines in each case correspond to the best fit to the data.

where I_b is the fluorescence intensity of bound *mant*-GTP and I_T is the total fluorescence intensity. A similar expression applies to free *mant*-GTP. Given eqs 14 and 16:

$$r = (I_f/I_T\nu_f r_f) + (I_b/I_T\nu_b r_b) \quad (17)$$

where I_f is the fluorescence intensity of free *mant*-GTP and ν_f is the fractional saturation of free *mant*-GTP. Since the sum of the fractions free (ν_f) and bound (ν_b) ligand is 1 and

$$I_T = I_f\nu_f + I_b\nu_b \quad (18)$$

employing eqs 13, 17, and 18, we obtain

$$\nu_b = (r - r_f)/[(r - r_f) + R(r_b - r)] \quad (19)$$

which is simplified to eq 15 when there is no change in the quantum yield ($R = 1$) (see also ref *47*, pp 308−309). Assuming one to one binding, applying an equivalent to eq 4 and eq 19, the following expression can be obtained:

$$r = (r_f + K_{mGTP}[P]_f R r_b)/(1 + K_{mGTP}[P]_f R) \quad (20)$$

The above equation was used, together with the previously obtained value of R and an equivalent of eq 3 to iteratively fit the r vs $[P]_f$ data, with different starting values of r_b and r_f, from which best-fitted values of K_{mGTP}, r_b, and r_f (which coincided with the measured value) were obtained. In complementary experiments apoFtsZ (375 nM) was titrated with increasing concentrations of *mant*-GTP. Fractional ligand saturation was obtained with eq 19 and multiplied times the *mant*-GTP concentration in the sample. The concentration of free *mant*-GTP ([*mant*-GTP]$_f$) was calculated with the equivalent to eq 8 employing *mant*-GTP concentrations. An equation equivalent to eq 5 was iteratively applied to fit the [*mant*-GTP]$_b$/[P]$_T$ vs [*mant*-GTP]$_f$ data to obtain the best-fitted values of n and K_{mGTP}.

Ligand Competition with mant-GTP. Samples (0.4 mL) were prepared containing a mixture of *mant*-GTP (final concentration 0.5 μM) and binding sites (final concentration 0.375 μM) and varying concentrations of a competing ligand in Pipes−Mg^{2+}. Samples with no competing ligand, with only *mant*-GTP, and with only buffer were included in each assay as controls. Fractional binding of *mant*-GTP was determined by fluorescence intensity and anisotropy as described above. Ligand affinities were determined using the same system of equations of the ligand competitions with ^{3}H-GTP (eqs 6−10), substituting $K_{^3H\text{-}GTP}$ with the previously obtained $K_{mant\text{-}GTP}$ and all ^{3}H-GTP concentrations with *mant*-GTP concentrations.

Determination of the Binding Affinities of the Reference Ligands ^{3}H-GTP and mant-GTP to ApoFtsZ. In order to set up an efficient fluorescence competition method to measure the binding of any ligands to the FtsZ nucleotide binding site, the equilibrium binding constants (K_b) of the reference ligands ^{3}H-GTP and *mant*-GTP to the nucleotide binding site of apoFtsZ were first measured. ^{3}H-GTP was titrated with apoFtsZ, and the reciprocal titrations of apoFtsZ with ^{3}H-GTP were also acquired (Figure 1A,B), giving fitted binding constants of $(2.84 \pm 0.36) \times 10^7$ M^{-1} and $(4.25 \pm 1.53) \times 10^7$ M^{-1}, respectively. The titration of apoFtsZ with ^{3}H-GTP also gave a number of binding sites $n = 0.77 \pm 0.07$, very close to that independently measured with *mant*-GTP after protein preparation (0.75 ± 0.04; see Experimental Procedures). The GTP binding constant chosen for the purposes of the subsequent competition assays was that obtained from the titration of ^{3}H-GTP with increasing concentrations of apoFtsZ. It was judged to be a more precise measurement due to better statistical fits and because the titration of apoFtsZ with ^{3}H-GTP gives less precise measurements at high ^{3}H-GTP concentrations, due to the very low proportion of [^{3}H-GTP]$_b$.

Binding titrations of *mant*-GTP with apoFtsZ and reciprocal titrations of apoFtsZ with *mant*-GTP were performed. Binding of *mant*-GTP to apoFtsZ causes a significant increase in its fluorescence emission intensity which, if not taken into account, can lead to the calculation of erroneous apparent K_b values when employing anisotropy measurements. This was quantified during the titrations of *mant*-GTP with apoFtsZ by acquiring the magic angle fluorescence intensity (I_M), which is directly proportional to the nonpolarized fluorescence intensity, in parallel to anisotropy measurements. From the intensity ratio between the bound and free fluorescence intensities acquired, an intensity coefficient ($R = 6.1 \pm 0.6$) was obtained and used to correct all anisotropy-based binding calculations. A $K_{mGTP} = (1.30 \pm 0.3) \times 10^6\ M^{-1}$ was also obtained from the intensity measurements (Figure 1C). Anisotropy measurements were obtained and used to plot titrations (Figure 1D). The anisotropy values obtained for free and bound *mant*-GTP were 0.027 ± 0.001 and 0.23 ± 0.01, respectively. The equilibrium binding constant obtained was $K_{mGTP} = (9.40 \pm 3.9) \times 10^5\ M^{-1}$. These results correct our previously reported K_{mGTP} values (*12*) by taking the intensity change of *mant*-GTP into consideration. Note that, unlike the titration using fluorescence intensities, because of the calculation due to the change in quantum yield between the bound and free form of *mant*-GTP, the $1/K_b$ value from the anisotropy measurements does not fit with the midpoint of the titration curve. Reciprocal experiments of titrating apoFtsZ (375 nM) against increasing concentrations of *mant*-GTP were also performed but gave large errors due to the lack of precision in measurements where the fraction of bound *mant*-GTP was very low (Supporting Information Figure S1A). We used the average K_{mGTP} value $9.40 \times 10^5\ M^{-1}$ as the reference for competition assays. K_{mGTP} reference values plus or minus the experimental error were also tested but gave systematically poor fits to the competition data. Fluorescence anisotropy was preferred due to its robustness compared to intensity measurements, which are more prone to interferences by light absorbing or fluorescent compounds.

For comparative purposes, *mant*-GDP was also titrated with apoFtsZ (Supporting Information Figure S1B). The free and bound anisotropy values were ~0.05 and ~0.29, respectively, and the $K_{mGDP} = (8.3 \pm 1.4) \times 10^5\ M^{-1}$. Thus, the ratio of K_{mGTP} to K_{mGDP}, is 1.13 ± 0.47.

RESULTS

Comparison of Fluorescent and ^{3}H-GTP Competition Methods for the Measurement of Ligand Binding Affinity to the Nucleotide Site of FtsZ. To validate the *mant*-GTP displacement method for the evaluation of ligands binding to the FtsZ nucleotide site, the binding affinities of six different ligands were measured through competition with ^{3}H-GTP and using the *mant*-GTP competition method, and the binding affinities obtained from both methods were compared (Figure 2, Table 1). Competition with *mant*-GTP gave accurate measurements of ligand binding with affinities from $10^3\ M^{-1}$ to nearly $10^8\ M^{-1}$. Binding constant values obtained through competition with *mant*-GTP were consistently somewhat higher than those obtained with ^{3}H-GTP (average 2.7 ± 1.1 times; Table 1). This offset is irrelevant for the purposes of comparing the affinities of different ligands among themselves. The *mant*-GTP competition method is able to detect ligands with a high K_b. However, this type of competition method is inaccurate for ligands with a binding affinity $\geq 10^2$ times higher than the probe (*46*), which includes the natural ligand GTP. Beyond this upper limit fittings for GTP were very similar for different theoretical binding affinities (6×10^8 to $10^{10}\ M^{-1}$, Figure 1A, dashed and gray traces). A working value of K_b for GTP for the purposes of comparison within the *mant*-GTP method was calculated from the $K_{GTP\text{-}^3H\text{-}GTP}$ value times the ratio factor

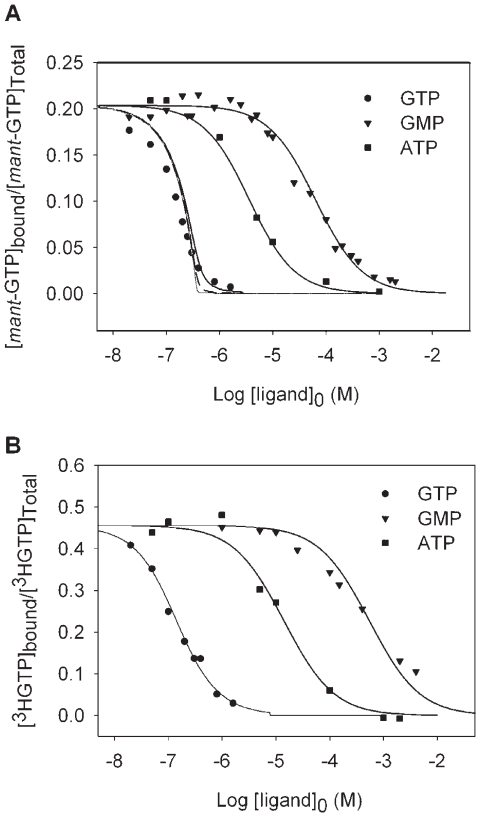

FIGURE 2: Comparison of ^{3}H-GTP and *mant*-GTP displacement results. Competition curves of GTP (circles), GMP (inverted triangles), and ATP (squares). Data were averaged from a minimum of two independent determinations. Solid lines correspond to the best fit to the competition data. (A) Displacement curves of *mant*-GTP (500 nM) from apoFtsZ (375 nM). For the GTP data, the solid, dashed, and gray traces are theoretical curves for 1×10^8, 6×10^8, and $1 \times 10^{10}\ M^{-1}$ K_b values, respectively. (B) Displacement curves of ^{3}H-GTP (100 nM) from apoFtsZ (75 nM).

Table 1: Binding Affinities of Nucleotides to FtsZ Determined with the ^{3}H-GTP and *mant*-GTP Competition Methods[a]

ligand	$K_{b(^3H\text{-}GTP)}$ (M^{-1})	$K_{b(mGTP)}$ (M^{-1})	$\Delta G_{(mGTP)}$ (kcal mol^{-1})
GTP	$(4.13 \pm 0.27) \times 10^7$	$(1.12 \pm 0.46) \times 10^8$	-10.98 ± 0.25
GDP		$\sim 3.8 \times 10^7$	~ -10.34
GMP	$(8.09 \pm 0.11) \times 10^3$	$(2.62 \pm 0.57) \times 10^4$	-6.02 ± 0.14
guanosine		$(3.42 \pm 0.37) \times 10^3$	-4.81 ± 0.07
PPP_i		$(4.16 \pm 0.01) \times 10^4$	-6.29 ± 0.01
PP_i	$(2.93 \pm 0.71) \times 10^4$	$(5.71 \pm 0.13) \times 10^4$	-6.48 ± 0.01
P_i		$(1.53 \pm 0.15) \times 10^3$	-4.34 ± 0.06
ATP	$(3.44 \pm 0.03) \times 10^5$	$(4.93 \pm 0.60) \times 10^5$	-7.76 ± 0.10
CTP	$(1.78 \pm 0.25) \times 10^5$	$(7.58 \pm 2.9) \times 10^5$	-8.01 ± 0.30
UTP	$(2.67 \pm 0.39) \times 10^5$	$(7.13 \pm 1.4) \times 10^5$	-7.98 ± 0.20

[a] $K_{b(^3H\text{-}GTP)}$, affinities obtained through ^{3}H-GTP competition; $K_{b(mGTP)}$, affinities obtained through *mant*-GTP competition; $\Delta G_{(mGTP)}$, binding free energy change calculated from $K_{b(mGTP)}$. GDP had a fitted equilibrium constant value ($\sim 1.1 \times 10^8\ M^{-1}$, Figure 3) that fell at the border the precise measurement range of the *mant*-GTP method, close to that of GTP. We know that GDP has a binding affinity 2.9 ± 0.5 times smaller that of GTP from the relative affinities previously obtained by direct methods, HPLC, and titration calorimetry (*12*). For consistency, we adopted a working value of $K_{bGDP\text{-}mGTP} = K_{bGTP\text{-}mGTP}/2.9 \approx 3.8 \times 10^7\ M^{-1}$. The binding affinities for GDP and GTP are respectively 2.3 and 2.9 times smaller than those previously reported employing *mant*-GTP displacement (*12*) due to the corrections now applied.

Table 2: Increment Free Energy Changes and Computationally Estimated Contributions to Binding of the Constituent Groups of GDP and GTP

group	ligand substitution	$\Delta\Delta G^\circ$ (kcal mol^{-1})	% $\Delta\Delta G^\circ$(GDP) experimental	% $E_{\text{MM-GBSA GDP}}$computed for 2VAP	% $\Delta\Delta G^\circ$(GTP) experimental	% $E_{\text{MM-GBSA GTP}}$computed for W15A-A, W15A-B
guanosine	$PPP_i \rightarrow$ GTP	−4.68	46	32	43	36, 47
guanine	XTP → GTP	∼−3.05	∼30	15	∼28	21, 12
ribose	$PPP_i \rightarrow$ XTP	∼−1.63	∼16	17	∼15	15, 35
phosphates	guanosine → GTP	−6.16	54	68	57	64, 53
α-phosphate	guanosine → GMP	−1.21	12	20	11	9, 4
	$P_i \rightarrow PP_i$	(−2.15)[a]	(21)[a]		(20)[a]	
β-phosphate	GMP → GDP	−4.32	42	48	40	34, 26
γ-phosphate	GDP → GTP	−0.64			6	21, 23
	$PP_i \rightarrow PPP_i$	(0.19)[a]			(−2)[a]	
∑groups		−10.85	100	100	100	100, 100

[a]These values are alternative free energy change calculations.

between binding affinities obtained by both methods. This gave $K_{\text{GTP-mGTP}} = (1.12 \pm 0.46) \times 10^8$ M^{-1} (Table 1).

The initial ligands tested with both methods included nucleotides different from GTP. Changing the base from guanine to adenine causes a predictable large drop in binding affinity (Table 1). Remarkably, changing the base to a pyrimidine (CTP or UTP) does not cause a further drop in the K_b (Table 1). One measurement of ADP binding through the *mant*-GTP competition method resulted in a K_b of 2.84×10^5 M^{-1}, making the $K_{\text{bATP}}/K_{\text{bADP}} = 1.74$. As in the case of *mant*-GTP and *mant*-GDP (see Experimental Procedures), the *γ*-phosphate had a weak effect on the observed binding affinity.

It should be noted that FtsZ from *M. jannaschii* does not polymerize at the temperature and concentrations employed in this study. Analytical ultracentrifugation results have indicated that it is a monomer under similar buffer conditions (*49*).

Binding Affinities of the Components of GTP to FtsZ Monomers. The binding affinities of the ligands that make up the parts of the nucleotide were determined employing the *mant*-GTP competition method (Figure 3A, Table 1). All of the GTP component ligands measured competed with *mant*-GTP for the FtsZ nucleotide binding site with a range of affinities between the nanomolar (GTP) and milimolar (P_i). Comparing the binding affinities of GDP and GTP (Table 1), the *γ*-phosphate has only a weak influence on the observed binding affinity. The *β*-phosphate clearly has a large weight in nucleotide interaction, as its removal drops affinity by 3 orders of magnitude, when comparing GDP to GMP (Table 1; uncorrected values in ref *12*). The α-phosphate, though not as important for binding as the *β*-phosphate, is also relevant, as its removal further drops affinity 1 order of magnitude, comparing GMP to guanosine (Table 1). Measurement of the phosphate components, P_i, PP_i, and PPP_i, revealed that they also compete with *mant*-GTP for the nucleotide binding site, with similar or higher affinities than guanosine (Table 1).

Calculation of incremental binding free energy changes ($\Delta\Delta G^\circ$) allows us to evaluate the apparent contributions of different parts of the nucleotide to FtsZ binding (Table 2). The $\Delta\Delta G^\circ$ value associated to the modification of a ligand gives a first approximation to the intrinsic binding free energy change of the added part of the molecule, assuming that everything else would remain the same (*50*−*52*). For example, the important contribution of the *β*-phosphate can be approximated as $\Delta\Delta G^\circ_{(\text{GMP}\rightarrow\text{GDP})} = \Delta G^\circ_{\text{GDP}} - \Delta G^0_{\text{GMP}} = -4.32$ kcal·mol^{-1}. The α-phosphate contributes −1.21 kcal·mol^{-1}. The apparent contribution of the *γ*-phosphate is at most −0.64 kcal/mol. The α- and *γ*-phosphate contributions can also be estimated from $\Delta\Delta G_{P_i\rightarrow PP_i}$ and $\Delta\Delta G_{PP_i\rightarrow PPP_i}$, respectively (Table 2), further supporting a negligible effect of the *γ*-phosphate on the observed binding. The guanosine contributes −4.68 kcal·mol^{-1}. Although the binding of guanine could not be directly measured due to low solubility (*53*), a tentative estimation of the contributions of guanine and ribose can be made by observing the very similar binding of non-guanine nucleotides (ATP, CTP, and UTP). If the non-guanine bases were not significantly contributing to binding, then $\Delta\Delta G^\circ_{(\text{NTP}\rightarrow\text{GTP})}$ and $\Delta\Delta G^\circ_{(PPP_i\rightarrow\text{NTP})}$ (where NTP is the nonguanine nucleotide) would give the contributions of guanine and ribose, which average −3.05 kcal·mol^{-1} and −1.63 kcal·mol^{-1}, respectively. If the non-guanine bases contribute to binding, then the actual contribution of ribose would be lower and that of guanine higher, assuming that the interactions made by the rest of the nucleotide did not change.

We can now compare the measured binding free energy changes for PPP_i, PP_i, and P_i (Table 1) to the estimated contributions of their corresponding parts of GTP (Table 2). $\Delta\Delta G_{\text{guanosine}\rightarrow\text{GTP}}$, which represents the contribution of the triphosphate moiety, is −6.16 kcal·mol^{-1}, very close to the measured binding free energy change of PPP_i. Binding of P_i and PP_i could occur in several positions on the nucleotide site. However, assuming a Boltzmann distribution with the *β*-phosphate position as the minimal energy state, we can calculate that >99% of P_i will bind in the *β* position. The observed binding affinity of P_i is very close to the estimated contribution of the *β*-phosphate to binding (−4.32 kcal·mol^{-1}). The observed binding affinity of PP_i is not very different from the contributions that can be estimated for each of the two possible diphosphate moieties, $\Delta\Delta G_{\text{guanosine}\rightarrow\text{GDP}} = \sim -5.53$ kcal·mol^{-1} and $\Delta\Delta G_{\text{GMP}\rightarrow\text{GTP}} = -4.96$ kcal·mol^{-1}. The ΔG° values of PPP_i and PP_i are similar.

Several crystal structures of FtsZs have shown an absence of nucleotide-induced conformational changes (*54*). The protein and bound nucleotides in the structures corresponding to our binding measurements above, the FtsZ monomers from *M. jannaschii* bound to GDP (PDB ID 2VAP) and to GTP-Mg^{2+} (from 1W5A), are practically superimposable (rmsd 0.62 Å), except for the presence of the *γ*-phosphate of GTP and Mg^{2+} that interact with loops T2, T3, and T4 of the FtsZ binding site (Figure 3B). Therefore, one may ask why these additional interactions do not translate into a markedly larger binding affinity of GTP over GDP in solution. This suggested compensatory changes in the system, which required a more detailed analysis.

Structural Analysis of GDP- and GTP-Bound FtsZ from Molecular Dynamics Trajectories. In order to pinpoint the precise interactions participating in nucleotide binding and to reveal potential conformational changes in solution, we first analyzed the results of 50 ns molecular dynamics simulations employing the

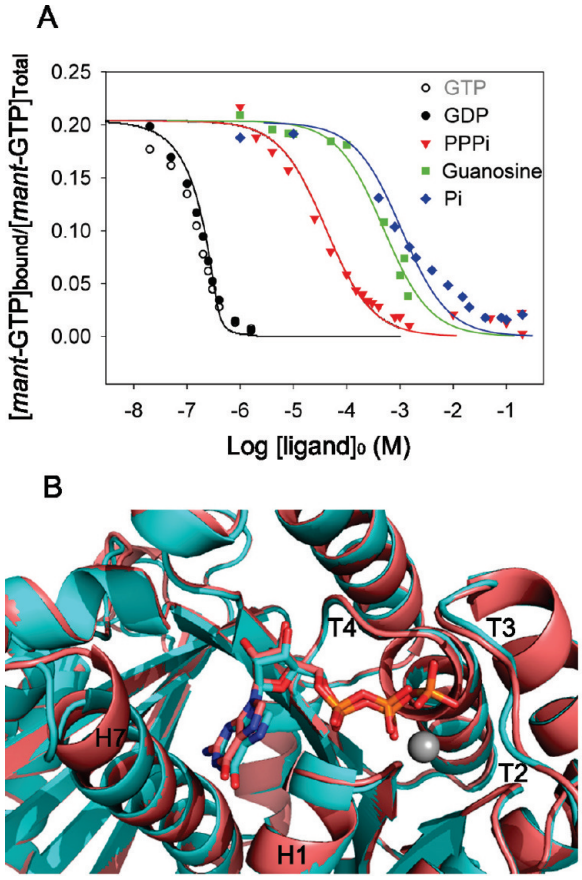

FIGURE 3: Binding of the constituent parts of GTP to FtsZ. (A) Displacement curves of *mant*-GTP (500 nM) from apoFtsZ (375 nM) employing GTP parts: GDP (black symbols), PPP_i (red), guanosine (green), and P_i (blue). GTP data (void circles) are included only for comparison with GDP. Data were averaged from a minimum of two independent determinations. Lines in each case correspond to the best competition fit. Resultant K_bs are in Table 1. (B) The nucleotide binding site in superimposed FtsZ monomers from *M. jannaschii* bound to GDP (PBB ID 2VAP, salmon) and to GTP-Mg^{2+} (1W5A-A, cyan). GDP and GTP are shown in colors by atom type and Mg^{2+} as a gray sphere.

crystal structures of FtsZ-GDP (2VAP) and FtsZ-GTP-Mg^{2+} (1W5A-A; see Experimental Procedures). The structural integrity of FtsZ protein with both ligands (GDP and GTP) is well conserved along the simulations (panels A and B of Figure 4 for GDP and GTP, respectively). For the ligand, two measurements were recorded. In the first one a fitting of each snapshot (to the minimized X-ray structures) was performed before rmsd calculation, yielding 1.28 ± 0.28 Å for GDP and 0.86 ± 0.20 Å for GTP, indicating that in both cases GDP/GTP conformation did not suffer major changes. In the second one no fitting was performed, monitoring the motion of the ligand within the binding site. The values were 2.28 ± 0.43 Å for GDP (Figure 4A) and 1.30 ± 0.12 Å for GTP (Figure 4B). The higher average value for GDP, as compared to GTP, indicates that GDP, being smaller than GTP, fluctuated more while finding its pose within the binding site.

Mass-weighted atomic positional fluctuations were calculated by residue along the entire trajectories and are shown in Figure 4C for FtsZ-GDP and Figure 4D for FtsZ-GTP. In addition to the very mobile N-terminal helix H0, the larger fluctuations (above 2 Å) correspond mainly to loop T3 (residues 98−103 with GDP and 97−100 with GTP), loop T5 (residues 164−169 with GDP), loop H6−H7 (residues 199−209 with GDP and 197−212 with GTP, including in both cases the top part of H7), loop S9−S10 (residues 325−328 with GDP and 325−331 with GTP), and loop S11−S12 (residues 347−352 with GDP).

The movements in the FtsZ molecule in the molecular dynamics simulations can be globally appreciated in Figure 4E (for 2VAP) and Figure 4F (1W5A-A), where minimized average structures after 50 ns are superimposed onto the X-ray ones. Average structures every 10 ns are superimposed in Supporting Information Figure S3. Loop T3 and the top part of H7 showed the largest structural variability, acting as the borders of the binding site where the GDP/GTP is accommodating. Globally similar results were obtained when FtsZ-GTP-Mg^{2+} was constructed by adding one Mg^{2+} ion to 1W5A-B in the same position as in chain A, with some local differences. Superposition of the initial and final binding sites showed significant displacements of GDP and GTP with respect to the crystal structures. The differences between the GDP and GTP-Mg^{2+} (for 1W5A-A and 1W5A-B) at the binding site after the full 50 ns trajectories are shown by Figure 4G,H. It can be appreciated how the accommodated nucleotides are no longer superimposable, in contrast to the initial crystal structures (Figure 3B). Interestingly, the GTP phosphates after molecular dynamics present a conformation resembling that found in the crystal structure of a W319Y FtsZ mutant (PDB entry 1W5E (*10*)).

Computational Analysis of GDP and GTP Binding to FtsZ. The individual interactions made by the guanine ring, ribose, and phosphates of GDP and GTP with their binding site along the molecular dynamics trajectories were inspected next. The interacting residues of FtsZ in 2VAP, 1W5A-A, and 1W5A-B are marked in Figure 5 (for earlier analyses of the interactions of GDP in the FtsZ crystal structure 1FSZ, see refs *6* and *9*).

The guanine ring is stacked between the side chains of F208 and A48, both in 2VAP and 1W5A-A (more weakly in 1W5A-B). F208 was replaced by K209 in 1W5A-A but not in 1W5A-B. The A48 interaction is shared with the α-phosphate in 2VAP, whereas in 1W5A this interaction is further shared with the ribose ring. There is also an electrostatic interaction with the carboxylic group of D212 in 1W5A-A, weakening along the trajectories of 1W5A-B and 2VAP. By contrast, for 1W5A-A a hydrogen bond forms between the carboxylic group of D212 and the hydrogen atom at position N1 or the hydrogen atoms from the amino group at position 2 (total occupancy only 19%). In 1W5A-B the N-terminal part of helix H7 bends inward, and D212 forms a hydrogen bond with N51. The nucleotide binding site gets somewhat narrower in 1W5A-B than in 1W5A-A. Both GDP and GTP present a weak hydrophobic interaction of the guanine ring with F162. Finally, two transient interactions (at 10 ns) were established with A211 and T159 in 2VAP, while in 1W5A (appearing at 20−30 ns and maintained thereafter) there is an electrostatic interaction with C129 and the interaction with T159.

The ribose ring in 2VAP presents a group of stable hydrophobic-driven interactions during the entire MD trajectory with P161, G130, L131 (also hydrogen bonded with occupancy of only 11%), with G132, and predominantly with R169 (shared with the two phosphate groups). In 1W5A-A, besides sharing the A48 hydrophobic interaction and part of the F208 electrostatic interactions with the guanine ring, the ribose ring also presents stable hydrophobic interaction during the entire MD trajectory with G130, L131, G132, and F162. Important interactions are a hydrogen bond formed between the E165 side chain (occupancy 68%) and the hydroxyl group at the 2′ position and an electrostatic interaction with R169. These two residues interact more closely with the ribose ring in 1W5A-B.

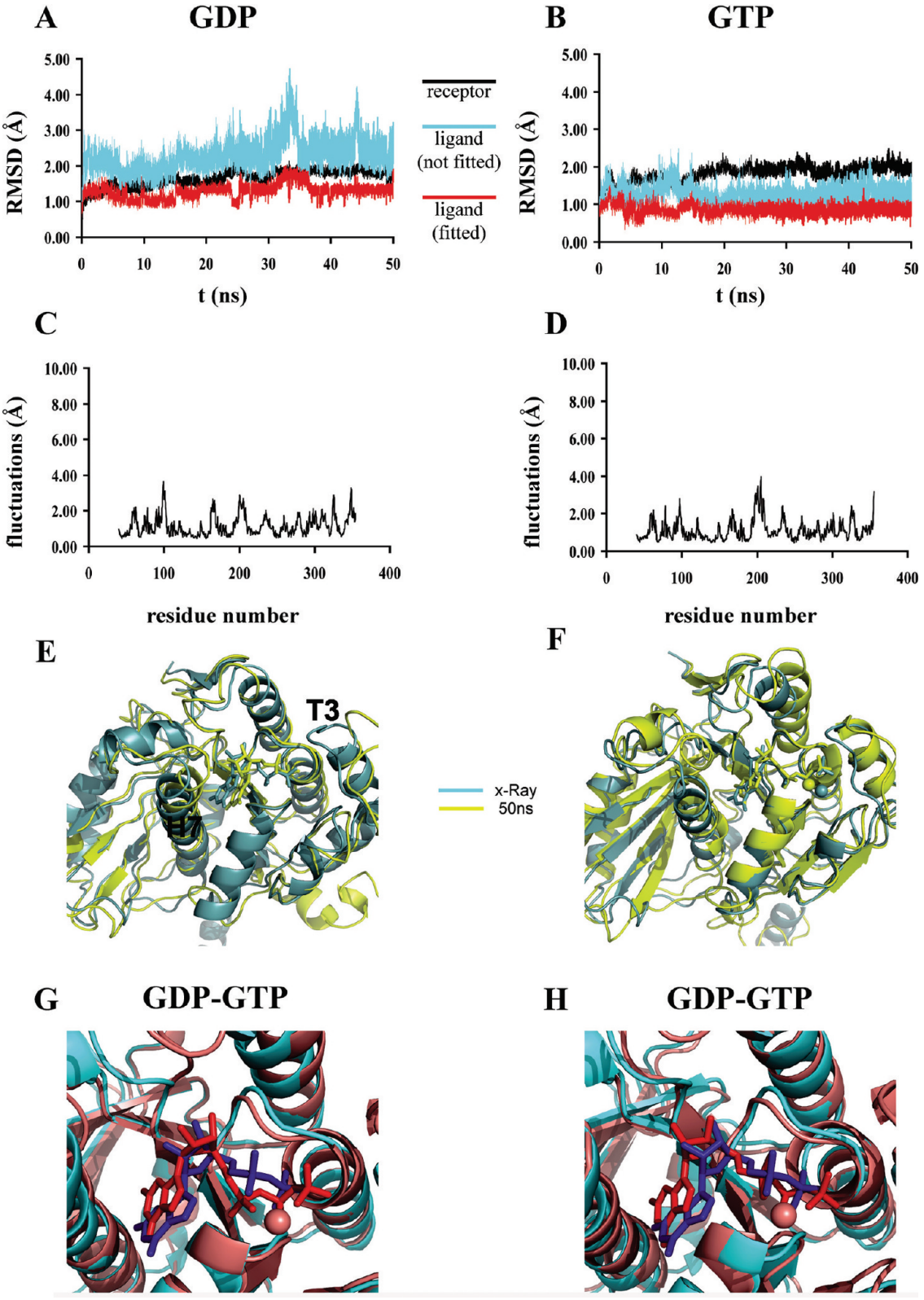

FIGURE 4: Molecular dynamics simulations of FtsZ-GDP and FtsZ-GTP-Mg^{2+}. (A) rmsd (in Å) along the MD simulation for FtsZ (black) and GDP (fitted in blue and not fitted in red) compared to the initial reference structure (2VAP; see text). (B) rmsd (in Å) along the simulation for FtsZ (black) and GTP (fitted in blue and not fitted in red) compared to the initial reference structure (1W5A-chain A). The rmsd of sampled snapshots (at 1 ps intervals) compared to the initial reference structures (the minimized X-ray structures) was measured. The average values obtained were 1.64 ± 0.22 Å with GDP (A) and 1.81 ± 0.22 Å with GTP (B). (C) Mass-weighted atomic positional fluctuations per residue along the trajectory for GDP (2VAP). (D) Mass-weighted atomic positional fluctuations per residue along the trajectory for GTP (1W5A). (E) Minimized average structures corresponding to the last 500 ps of the 50 ns MD (yellow) superimposed onto the minimized X-ray one (blue) for GDP (2VAP). (F) A similar comparison for GTP (1W5A). The average structures at each 10 ns are available as Supporting Information Figure S3. (G) Differences between GDP (cyan) and GTP-Mg^{2+} (salmon, IW5A-A) at the binding sites after the full 50 ns trajectories. GDP and GTP are shown in blue and red, respectively. Mg^{2+} is shown as a sphere. (H) Differences between GDP (cyan) and GTP-Mg^{2+} (salmon, 1W5A-B) at the binding sites after the full 50 ns trajectories.

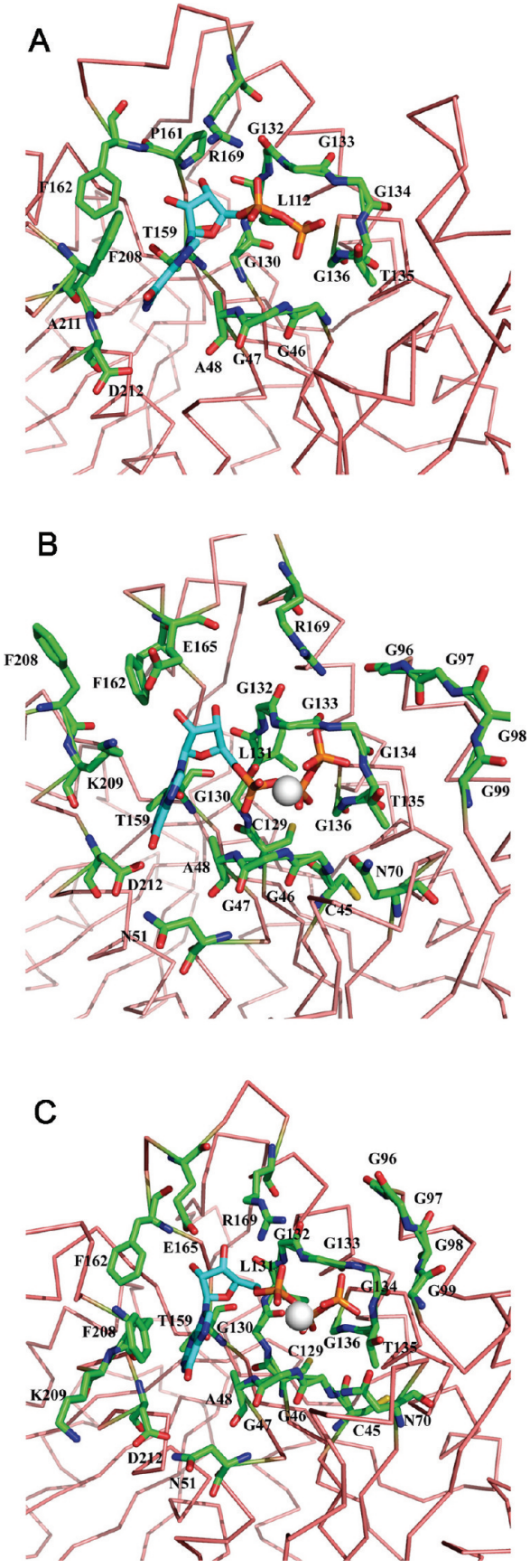

FIGURE 5: Interactions of FtsZ with GDP and GTP after molecular dynamics. (A) GDP-FtsZ interacting residues shown in sticks and colored according to atom types after 50 ns MD from the crystal structure 2VAP. (B) GTP-FtsZ interacting residues after MD of 1W5A-chain A. Mg^{2+} is shown as a small white sphere. (C) GTP-FtsZ interacting residues after MD of 1W5A-chain B.

The α-phosphate group in 2VAP interacts with A48 forming a hydrogen bond that is lost at the end of the simulation, becoming a moderate hydrophobic interaction. It also forms a double hydrogen bond between the R169 side chain and the O2 oxygen atom from GDP which is maintained during the whole trajectory (occupancy 48%). Finally, a relatively strong electrostatic interaction is established with G133, which is also shared with the *β*-phosphate group. In 1W5A-A the α-phosphate group interacts through a hydrophobic interaction with G47 (whereas the electrostatic interaction is assigned to the *β*-phosphate group), an electrostatic interaction with A48 (whereas the hydrophobic interaction was assigned to the ribose ring; see above), and an electrostatic interaction with G133 (shared with both phosphate groups at *β* and *γ* positions).

The *β*-phosphate group interacts similarly in GDP and GTP. It is attached to the protein in 2VAP mainly through hydrogen bond interactions with G134 (occupancy 27%), T135 (main and side chains, 21 and 67% occupancy, respectively), G136 (occupancy 33%), and G47 (transient, van der Waals interaction is shared with the α-phosphate group). Minor interactions are established with G46 (electrostatic) and G90 (weak electrostatic). In a similar way, the *β*-phosphate group in 1W5A-A is attached to the protein through hydrogen bond interactions with G134 (occupancy 21%) and G136 (occupancy 29%), electrostatic interactions with G46 and G47, hydrophobic interaction with T135, and the shared interaction with G133 with the other two phosphate groups. Minor interactions are established with C45 and N70.

Finally, the *γ*-phosphate group in the 1W5A-A complex is attached to the protein through two hydrogen bond interactions established with T135 (both main and side chains with occupancies 29 and 84%, respectively) and the shared interaction with G133. The initial hydrogen bond interactions found in the X-ray structure with the T3 loop through G96, A97, G98, and G99 residues are lost (1W5A-A) or reduced significantly (1W5A-B) during the MD trajectory.

The free energies of binding between GDP/GTP and FtsZ were calculated by means of the MM-GBSA method (for the enthalpic part) and quasiharmonic analysis (for the entropic part) (see Experimental Procedures). The MM-GBSA energies were stable by the end of the trajectories (Supporting Information Figure S2). The average values (and standard deviations) over the last 500 ps for each period of 10 ns are collected in Supporting Information Table S2 (for GDP) and Table S3 (for GTP). The MM-GBSA energy values were further partitioned into individual residue contributions to allow for a finer analysis. It should be noted that MM-GBSA energy values for individual residues (as implemented in the AMBER 10 package) are the binding energies assigned by the force field to the residues being considered within the complex and not really binding free energy changes, that is, the values resulting from subtracting, from the complex energy, the energies corresponding to the isolated receptor and ligand. This shortcoming considered, the individual interactions (Supporting Information Table S4 for GDP and Table S5 for GTP) were assigned to the different parts of the GDP/GTP molecules after visual inspection. Their relative contributions to GDP/GTP binding energy along the MD trajectories were collected (Supporting Information Table S6 for GDP and Table S7 for GTP).

GDP makes numerous contacts with FtsZ upon binding, but our computational analysis indicated that the interactions between the α- and *β*-phosphate and amino acids G132, G133, G134 at loop T4 and R169 at loop T5 (Figure 5) account for a large part of the GDP binding energetics, with roughly half of the free energy concentrated on the interaction between these key

residues and the phosphates. By the end of the molecular dynamics runs, the resulting contribution of the guanine ring to the GDP (2VAP) and GTP (1W5A) interactions affords average values of 15% and 12−21% of the total free energy change, respectively (Table 2). The average contribution of the ribose ring is 17% in GDP and 15−35% in GTP. The contribution of the α-phosphate is 20% in GDP and 4−9% in GTP. There is a dominant contribution of the *β*-phosphate, 48% in GDP and 26−34% in GTP (34−44% if the *γ*-phosphate was removed). These computed binding energy percentages showed correlation with the experimentally estimated group incremental free energy change $\Delta\Delta G$ values (Table 2). The exception is the *γ*-phosphate group, which according to these calculations contributes about 21−23% of the binding free energy of GTP but a maximum of 6% of the total experimental $\Delta\Delta G$ (Table 2).

The discrepancy between the significant interactions made by the *γ*-phosphate of GTP in the structure of the complex with FtsZ (both in the crystal structure and after molecular dynamics simulations) with the very weak affinity increase of GTP with respect to GDP may be ascribed to different interactions made by the rest of the nucleotide, as in the molecular dynamics simulations. These differences practically compensate for the binding of the *γ*-phosphate. In this case $\Delta\Delta G$ is not a valid approximation to the intrinsic free energy change of the added group.

Interactions of Inhibitory C8 Derivatives of GTP with FtsZ. A series of GTP analogues with small substituents at C8 of the guanine base have been shown to inhibit the polymerization of FtsZ as monitored by 90° light scattering, while supporting the *in vitro* assembly of the eukaryotic analogue of FtsZ, tubulin (*26*). They served as a proof of concept that it is possible to specifically target compounds to the nucleotide binding site of purified FtsZ without inhibiting eukaryotic tubulin. The detailed measurements of affinity for the GTP binding site of FtsZ and their inhibitory capacity are reported here (Figure 6 and Table 3), as a test of the *mant*-GTP competition method. One of the compounds, 8-methoxy-GTP (MeOGTP), had an affinity similar to that of GTP, which could be approximated to $K_b \approx 1.6 \times 10^8\ M^{-1}$. The compound with the second highest affinity, 8-pyrrolidino-GTP (PyrrGTP), presented a K_b half of that of GTP, $(5.2 \pm 1.4) \times 10^7\ M^{-1}$. 8-Cl-GTP (ClGTP), 8-Br-GTP (BrGTP), 8-I-GTP (IGTP), and 8-*tert*-butyl-GTP (*t*BuGTP) had intermediate K_b values (between 1×10^7 and $1.8 \times 10^7\ M^{-1}$). Finally, there was one compound, 8-morpholino-GTP (MorphGTP), with a K_b of $(2.31 \pm 0.04) \times 10^6\ M^{-1}$. It appears that the presence of more bulky substitutions at C8 leads to lesser affinity for the nucleotide binding site. These measurements (Figure 6A and Table 3) complement previous K_b measurements (*26*), also including corrected calculations due to the quantum yield change of *mant*-GTP upon binding (see Experimental Procedures). We also measured the inhibition of FtsZ assembly by the compounds with a FtsZ pelleting assay, which determines the concentration of polymerized FtsZ, giving more reliable quantitative results than 90° light scattering. Four compounds representing every K_b group (MeOGTP, PyrrGTP, BrGTP, and MorphGTP) were assayed to determine their polymerization IC_{50}. The pelleting assays confirmed that the log IC_{50} linearly correlates to the log K_d of the compounds (Figure 6B) with FtsZ both from *E. coli* and from *B. subtilis*. This supports the use of stable apoFtsZ from *M. jannaschii* as an experimental model of the FtsZ nucleotide binding site.

Applying the mant-GTP Competition Assay To Screen Natural and Synthetic Compounds for Binding to the FtsZ Nucleotide Site. The nucleotide binding site of FtsZ is a good candidate for the search of novel compounds that could specifically inhibit bacterial cell division and therefore act as potential new antibiotics. Compounds should be of a different chemistry to the natural nucleotides in order to be effective antibiotics. Sanguinarine, cinnamaldehyde, and totarol are compounds that have been reported to inhibit FtsZ activity (*21*−*23*), but they did

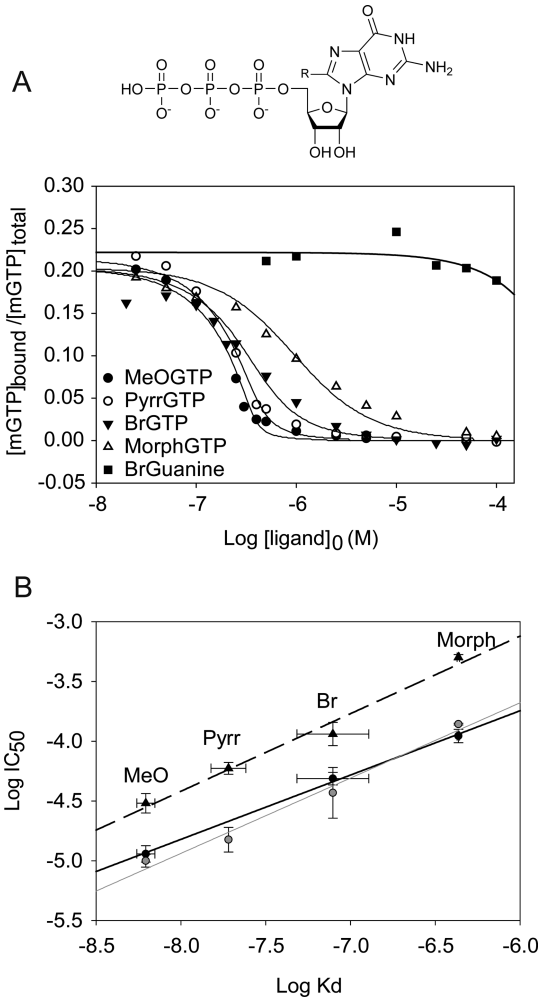

FIGURE 6: Affinity for the nucleotide site and FtsZ assembly inhibition by GTP derivatives substituted at C8. (A) Displacement curves of *mant*-GTP (500 nM) from apoFtsZ (375 nM) employing GTP derivatives: MeOGTP (solid circle), PyrrGTP (empty circle), BrGTP (solid inverted triangle), MorphGTP (empty triangle), and BrGuanine (square). Lines in each case correspond to the best fit to the competition curve. (B) Correlation of log K_d with log IC_{50} of polymerization using FtsZ from *B. subtilis* (triangles) and *E. coli* (black circles) and correlation of log K_d to previously reported (*26*) polymerization IC_{50} of FtsZ from *E. coli* measured by light scattering (gray circles). Data were averaged from a minimum of two independent determinations. Lines in each case correspond to the best linear fit.

Table 3: Binding Affinities of C8-Substituted GTP Analogues to FtsZ Determined with the *mant*-GTP Competition Method

ligand	K_b (M^{-1})	$\Delta G°$ (kcal mol^{-1})
MeOGTP	$\sim 1.6 \times 10^8$	~ -11.2
PyrrGTP	$(5.24 \pm 1.4) \times 10^7$	-10.52 ± 0.19
ClGTP	$(1.01 \pm 0.05) \times 10^7$	-9.55 ± 0.03
BrGTP	$(1.27 \pm 0.80) \times 10^7$	-9.68 ± 0.58
IGTP	$(1.81 \pm 0.48) \times 10^7$	-9.89 ± 0.18
tBuGTP	$(1.01 \pm 0.08) \times 10^7$	-9.54 ± 0.05
MorphGTP	$(2.31 \pm 0.04) \times 10^6$	-8.67 ± 0.01
BrGuanine	$< 1 \times 10^4$	> -5.45

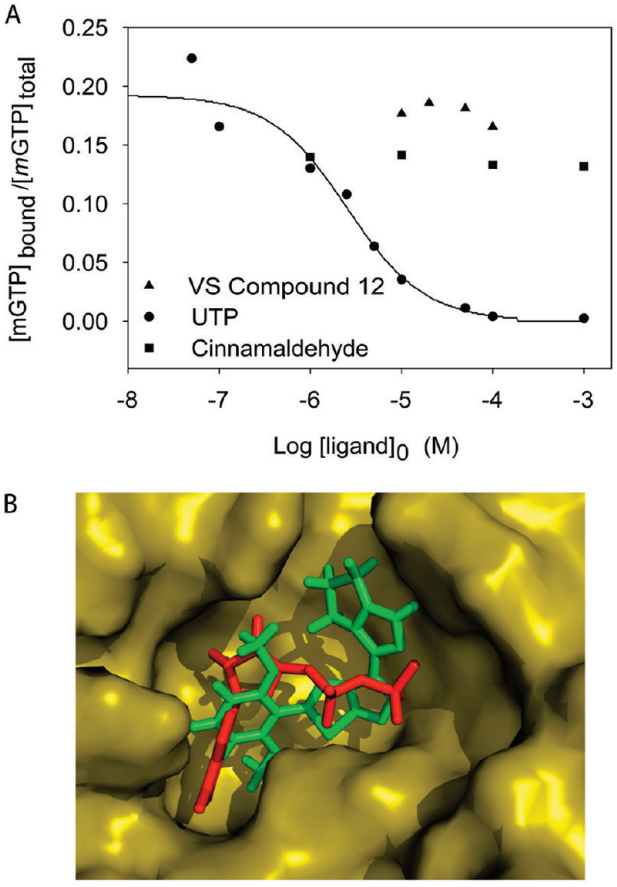

FIGURE 7: Examples of results obtained with nonnucleotide compounds. (A) Competition experiment with cinnamaldehyde (squares) and virtual screening compound **12** (triangles, Supporting Information Table S9) compared to UTP (circles; the line corresponds to the best competition fit). (B) Docking model of compound **12** (green, Supporting Information Table S9) superimposed to GDP (red) at the nucleotide binding site.

not displace *mant*-GTP within the concentration range measured (representative competition assay example in Figure 7A), indicating that they should bind to another site in FtsZ. We had previously found that the FtsZ polymer stabilizing agent PC190723 binds to a site different from the nucleotide site (*25*).

An alternative to known and natural compounds is the use of small molecules from large synthetic libraries. To narrow down the search, we directly employed a virtual screening method on the structure of bacterial FtsZ from the opportunistic pathogen *P. aeruginosa*, based on the conservation of the nucleotide binding site. The procedure consisted in docking and rescoring with molecular dynamics and MM-GBSA binding energy analysis [(*38*); see Experimental Procedures]. The first VS round was performed using the ChemBridge library, ending up with 100 molecules sorted by their binding energies as obtained from the MD trajectories. After visually inspecting their simulated complexes with FtsZ, chemical features, and predicted solubility (*55*), 17 compounds were selected for experimental tests (Supporting Information Table S8). Most of them had severe solubility problems. Since no active molecules were found, we used a different chemical library from IBScreen, selecting compounds predicted to be more soluble. Again, and despite good predicted docking and computed binding energies (Supporting Information Table S9), the finally selected 19 compounds still did not compete with *mant*-GTP for binding to FtsZ (Figure 7) nor inhibited assembly of bacterial FtsZ from *E. coli*. It should be noted that practical solubility was generally poor with respect to predicted solubility, making the evaluation of many compounds at high concentrations impossible.

DISCUSSION

In this study we first devised and validated a fluorescence polarization method for assaying ligand binding to the nucleotide site in FtsZ and measuring their affinities. We have employed this method to gain insight into the interaction of GDP/GTP with their binding site in FtsZ monomers. We were able to assign the relative contribution of each part of the nucleotides to the total interaction, that were compared with the results from MM-GBSA analysis after long molecular dynamics trajectories (50 ns) simulating FtsZ with GDP/GTP bound. In addition, we measured the K_b for a series of C8-GTP derivatives and directly measured their inhibitory capacity on FtsZ polymerization. We also tested several previously reported FtsZ inhibitors and compounds from virtual screening for potential binding to the nucleotide site.

Competition assays with a selection of nucleotide ligands showed that the *mant*-GTP method gives reliable measurements of K_b, though slightly higher than those obtained with a ^{3}H-GTP competition method. Competition with *mant*-GTP can efficiently measure ligands with binding affinities below 10^8 M^{-1} and gives reliable results after even 7 h at 25 °C (data not shown). The *mant*-GTP measurements are scalable to medium- or high-throughput screening assays employing plate readers, whereas the ^{3}H-GTP method can be preferably employed to manually counterscreen a smaller number of samples.

We employed the *mant*-GTP competition method to test for binding to the nucleotide site several FtsZ-interacting compounds with chemistries very different from nucleotides [sanguinarine (*21*), cinnamaldehyde (*22*), totarol (*23*), PC190723 (*24*, *25*)]. We also tested a total of 36 compounds from two successive virtual screening rounds, with negative results. Among potential causes, low solubility of the VS compounds frequently made testing at high concentrations impossible, so an improvement on the solubility prediction algorithms employed may be necessary. Another possibility would be to test VS on relaxed FtsZ structures after long molecular dynamics trajectories (discussed below). In addition, the FtsZ nucleotide binding site is highly exposed to the solvent, representing a challenge to current docking and scoring schemes. Our *mant*-GTP competition method would be suited to analyze the binding of compounds directed to the GTP site of FtsZ, such as PC170942, PC58538 (*56*), and the chrysophaentins (*57*).

Employing C8-substituted analogues of GTP, we found a linear relationship between the log K_b and the log IC_{50} of polymerization of FtsZ from *E. coli* and *B. subtilis*. This confirms but also improves upon previously reported results (*26*). The affinities of 8-Cl-GTP and 8-Br-GTP relative to GTP are compatible with recent free energy calculations, which take into account the effect of these substitutions in the dihedral angle distribution around the glycosidic bond (*58*). The results demonstrate that our method of measurement of modified nucleotides binding to the GTP site in FtsZ can serve to predict inhibitory effects on FtsZ polymerization.

We obtained insight into the interactions of FtsZ with GTP through competition measurements with the nucleotide and its components. Incremental free energy changes were employed to estimate, in a first approximation, group contributions to binding. Guanosine was estimated to contribute less than half the binding energy of GDP, distributed between the guanine and

ribose moieties (Table 2). These measurements indicated that the β-phosphate provides the dominant interaction, accounting for 42% of total binding free energy change, with the α-phosphate contributing 12%. The binding free energy changes of P_i, PP_i, and PPP_i measured independently were compatible with the dominant nature of the β-phosphate interaction. The binding free energy change of P_i was compatible with predominant binding to the β-phosphate locus.

Curiously, adding the incremental free energy changes of the parts of the nucleotide makes up the observed free energy change of the complete nucleotide. The observed (Table 1) and the incremental free energy changes (Table 2) for guanosine and the phosphates are practically coincident. This is puzzling because taking $\Delta\Delta G$ as an estimate of the intrinsic contact free energy change, a minimal difference $\Delta G^\circ_{obs} - \Delta\Delta G \approx 2.4$ kcal·mol^{-1} is expected, coming from the change in entropy of mixing in a bimolecular reaction, which does not count in the unimolecular binding of a part of the ligand (*50*). Lacking such systematic difference from intrinsic to observed free energy changes suggests compensatory effects of solvation and conformational or mobility differences.

Computational analysis through molecular dynamics and MM-GBSA binding energy calculations, although not a strictly comparable method, supported the importance of the phosphate groups in GDP binding, predicting relative contributions close to the experimental incremental free energy changes. It also predicted relatively modest contributions by the guanine and ribose moieties (see comparison in Table 2).

The binding affinities of triphosphate nucleotides were only slightly higher than those obtained for the analogous diphosphate nucleotides; thus the incremental free energy change resulting from adding the γ-phosphate is strikingly close to zero. It could be thought that the γ-phosphate has an irrelevant contribution to the binding energy of GTP. However, the γ/β-phosphate signal is very important in FtsZ dynamics, as FtsZ polymerizes in the presence of GTP and GDP triggers disassembly. It has been hypothesized that GTP facilitates a "straight" conformation favorable to polymer assembly while GDP favors a "curved" conformation that destabilizes FtsZ polymers (*45*). But our experimental results show that FtsZ monomers do not significantly favor GTP over GDP binding. Computational analysis of binding offers a possible explanation. The γ-phosphate makes strong interactions with the nucleotide site. The crystal structures of FtsZ-GDP and -GTP complexes are very similar, but upon molecular dynamics simulations the interactions of other parts of the GTP nucleotide also change in comparison with GDP, including the guanine ring and the α-phosphate. For GDP the main differences observed upon molecular dynamics simulation were the guanine ring losing a hydrogen bond with the side chain of D212, forming instead a double hydrogen bond with N51. Other contributions implying the guanine ring are associated with the weakening of A48 and F208 interactions, which allows GDP to perform a small displacement, optimizing the α-phosphate−R169 interaction. For GTP, the computational results show that in spite of several changes its five moieties maintain their resultant interaction energies along the trajectory. The γ-phosphate is tightly bound to FtsZ through hydrogen bond interactions with G133 and T135, contributing 21−23% of the total GTP-FtsZ binding energy. Consequently, the numerical value $\Delta\Delta G_{GDP\rightarrow GTP}$ is not the intrinsic contribution of the γ-phosphate to binding; therefore, the percent $\Delta\Delta G$ that can be calculated for this part of GTP deviates more from the computational estimates. The FtsZ homologue tubulin also presents an only slightly higher affinity for GTP than for GDP at its exchangeable site in the presence of magnesium (*59*). However, other GTPase proteins show different affinities (*60*, *61*).

The differences between the MD simulations and the crystal structures may be taken as suggesting the presence of average conformations in solution different from a frozen conformation in the crystal structures or only as indications of potential movements in the FtsZ structure. Differences between FtsZ-GDP and FtsZ-GTP, which were not observed in the corresponding crystal structures, are predicted by the molecular dynamics simulations. They suggest that, upon GTP hydrolysis to GDP and P_i release following FtsZ assembly, not only are the interactions of the γ-phosphate and the coordinated magnesium lost but the GDP may accommodate in the binding site establishing different interactions, which might also trigger the FtsZ disassembly switch (*17*). Obviously, the different effect of GTP and GDP on FtsZ polymer stability may also be due to the added interactions between the γ-phosphate and the next monomer in a FtsZ filament (*10*, *11*), which should bind GTP and GDP with different affinities (*12*) than the FtsZ model monomer employed in this work.

Taken together, our results give insight into the precise nature of the interactions between GTP and the nucleotide binding site of FtsZ. The fluorescent method developed permits detecting and analyzing the binding of any ligand replacing GTP in FtsZ monomers. The new information obtained could be useful in the rational design of new compounds targeting the nucleotide binding site of FtsZ. In particular, compounds could be designed to specifically interact with the FtsZ residues with the most important contributions to nucleotide binding, especially compounds mimicking the β- and γ-phosphate groups.

ACKNOWLEDGMENT

We thank Maria A. Oliva for helpful discussion and David Juan for technical assistance.

SUPPORTING INFORMATION AVAILABLE

Table of FtsZ inhibitors (S1), tables of MM-GBSA energies (S2−S7), tables of virtual screening compounds (S8 and S9), Figures S1−S3, and PDB files with average structures from molecular dynamics. This material is available free of charge via the Internet at http://pubs.acs.org.

REFERENCES

1. Bi, E., and Lutkenhaus, J. (1991) FtsZ ring structure associated with division in *Escherichia coli*. *Nature 354*, 161–164.
2. Ma, X. L., Ehrhardt, D. W., and Margolin, W. (1996) Colocalization of cell division proteins FtsZ and FtsA to cytoskeletal structures in living *Escherichia coli* cells by using green fluorescent protein. *Proc. Natl. Acad. Sci. U.S.A. 93*, 12998–13003.
3. Hale, C. A., and deBoer, P. A. J. (1997) Direct binding of FtsZ to ZipA, an essential component of the septal ring structure that mediates cell division in *E. coli*. *Cell 88*, 175–185.
4. Pichoff, S., and Lutkenhaus, J. (2005) Tethering the Z ring to the membrane through a conserved membrane targeting sequence in FtsA. *Mol. Microbiol. 55*, 1722–1734.
5. Osawa, M., Anderson, D. E., and Erickson, H. P. (2008) Reconstitution of contractile FtsZ rings in liposomes. *Science 320*, 792–794.
6. Löwe, J., and Amos, L. A. (1998) Crystal structure of the bacterial cell-division protein FtsZ. *Nature 391*, 203–206.
7. Nogales, E., Wolf, S. G., and Downing, K. H. (1998) Structure of the alpha beta tubulin dimer by electron crystallography. *Nature 393*, 191–191.
8. Erickson, H. P. (2007) Evolution of the cytoskeleton. *BioEssays 29*, 668–677.

9. Nogales, E., Downing, K. H., Amos, L. A., and Löwe, J. (1998) Tubulin and FtsZ form a distinct family of GTPases. *Nat. Struct. Biol. 5*, 451–458.
10. Oliva, M. A., Cordell, S. C., and Löwe, J. (2004) Structural insights into FtsZ protofilament formation. *Nat. Struct. Mol. Biol. 11*, 1243–1250.
11. Scheffers, D. J., de Wit, J. G., den Blaauwen, T., and Driessen, A. J. M. (2002) GTP hydrolysis of cell division protein FtsZ: Evidence that the active site is formed by the association of monomers. *Biochemistry 41*, 521–529.
12. Huecas, S., Schaffner-Barbero, C., Garcia, W., Yebenes, H., Palacios, J. M., Diaz, J. F., Menendez, M., and Andreu, J. M. (2007) The interactions of cell division protein FtsZ with guanine nucleotides. *J. Biol. Chem. 282*, 37515–37528.
13. Chen, Y. D., and Erickson, H. P. (2009) FtsZ filament dynamics at steady state: Subunit exchange with and without nucleotide hydrolysis. *Biochemistry 48*, 6664–6673.
14. Huecas, S., Llorca, O., Boskovic, J., Martin-Benito, J., Valpuesta, J. M., and Andreu, J. M. (2008) Energetics and geometry of FtsZ polymers: Nucleated self-assembly of single protofilaments. *Biophys. J. 94*, 1796–1806.
15. Dajkovic, A., Mukherjee, A., and Lutkenhaus, J. (2008) Investigation of regulation of FtsZ assembly by SulA and development of a model for FtsZ polymerization. *J. Bacteriol. 190*, 2513–2526.
16. Miraldi, E. R., Thomas, P. J., and Romberg, L. (2008) Allosteric models for cooperative polymerization of linear polymers. *Biophys. J. 95*, 2470–2486.
17. Martin-Galiano, A. J., Buey, R. M., Cabezas, M., and Andreu, J. M. (2010) Mapping flexibility and the assembly switch of cell division protein FtsZ by computational and mutational approaches. *J. Biol. Chem. 285*, 22554–22565.
18. Vollmer, W. (2006) The prokaryotic cytoskeleton: A putative target for inhibitors and antibiotics? *Appl. Microbiol. Biotechnol. 73*, 37–47.
19. Lock, R. L., and Harry, E. J. (2008) Cell-division inhibitors: New insights for future antibiotics. *Nat. Rev. Drug Discov. 7*, 324–338.
20. Margalit, D. N., Romberg, L., Mets, R. B., Hebert, A. M., Mitchison, T. J., Kirschner, M. W., and RayChaudhuri, D. (2004) Targeting cell division: Small-molecule inhibitors of FtsZ GTPase perturb cytokinetic ring assembly and induce bacterial lethality. *Proc. Natl. Acad. Sci. U.S.A. 101*, 13969–13969.
21. Beuria, T. K., Santra, M. K., and Panda, D. (2005) Sanguinarine blocks cytokinesis in bacteria by inhibiting FtsZ assembly and bundling. *Biochemistry 44*, 16584–16593.
22. Domadia, P., Swarup, S., Bhunia, A., Sivaraman, J., and Dasgupta, D. (2007) Inhibition of bacterial cell division protein FtsZ by cinnamaldehyde. *Biochem. Pharmacol. 74*, 831–840.
23. Jaiswal, R., Beuria, T. K., Mohan, R., Mahajan, S. K., and Panda, D. (2007) Totarol inhibits bacterial cytokinesis by perturbing the assembly dynamics of FtsZ. *Biochemistry 46*, 4211–4220.
24. Haydon, D. J., Stokes, N. R., Ure, R., Galbraith, G., Bennett, J. M., Brown, D. R., Baker, P. J., Barynin, V. V., Rice, D. W., Sedelnikova, S. E., Heal, J. R., Sheridan, J. M., Aiwale, S. T., Chauhan, P. K., Srivastava, A., Taneja, A., Collins, I., Errington, J., and Czaplewski, L. G. (2008) An inhibitor of FtsZ with potent and selective anti-staphylococcal activity. *Science 321*, 1673–1675.
25. Andreu, J. M., Schaffner-Barbero, C., Huecas, S., Alonso, D., Lopez-Rodriguez, M. L., Ruiz-Avila, L. B., Nunez-Ramirez, R., Llorca, O., and Martin-Galiano, A. J. (2010) The antibacterial cell division inhibitor PC190723 is a FtsZ polymer stabilizing agent which induces filament assembly and condensation. *J. Biol. Chem. 285*, 14239–14246.
26. Läppchen, T., Pinas, V. A., Hartog, A. F., Koomen, G. J., Schaffner-Barbero, C., Andreu, J. M., Trambaiolo, D., Löwe, J., Juhem, A., Popov, A. V., and den Blaauwen, T. (2008) Probing FtsZ and tubulin with C8-substituted GTP analogs reveals differences in their nucleotide binding sites. *Chem. Biol. 15*, 189–199.
27. Läppchen, T., Hartog, A. F., Pinas, V. A., Koomen, G. J., and den Blaauwen, T. (2005) GTP analogue inhibits polymerization and GTPase activity of the bacterial protein FtsZ without affecting its eukaryotic homologue tubulin. *Biochemistry 44*, 7879–7884.
28. Vollmer, W. (2008) Targeting the bacterial Z-ring. *Chem. Biol. 15*, 93–94.
29. Gordon, J. C., Myers, J. B., Folta, T., Shoja, V., Heath, L. S., and Onufriev, A. (2005) H++: A server for estimating pKas and adding missing hydrogens to macromolecules. *Nucleic Acids Res. 33*, W368–W371.
30. Honig, B., and Nicholls, A. (1995) Classical electrostatics in biology and chemistry. *Science 268*, 1144–1149.
31. Wang, J. M., Cieplak, P., and Kollman, P. A. (2000) How well does a restrained electrostatic potential (RESP) model perform in calculating conformational energies of organic and biological molecules? *J. Comput. Chem. 21*, 1049–1074.
32. Jorgensen, W. L., Chandrasekhar, J., Madura, J. D., Impey, R. W., and Klein, M. L. (1983) Comparison of simple potential functions for simulating liquid water. *J. Chem. Phys. 79*, 926–935.
33. Case, D. A., Darden, T. A., Cheatham, T. E., Simmerling, C. L., Wang, J., Duke, R. E., Luo, R., Crowley, M., Walker, R. C., Zhang, W., Merz, K. M., Wang, B., Hayik, S., Roitberg, A., Seabra, G., Kolossváry, I., Wong, K. F., Paesani, F., Vanicek, J., Wu, X., Brozell, S. R., Steinbrecher, T., Gohlke, H., Yang, L., Tan, C., Mongan, J., Hornak, V., Cui, G., Mathews, D. H., Seetin, M. G., Sagui, C., Babin, V., and Kollman, P. A. (2008) AMBER 10, University of California, San Francisco.
34. Humphrey, W., Dalke, A., and Schulten, K. (1996) VMD: Visual molecular dynamics. *J. Mol. Graphics 14* (33−38), 27–38.
35. Kollman, P. A., Massova, I., Reyes, C., Kuhn, B., Huo, S. H., Chong, L., Lee, M., Lee, T., Duan, Y., Wang, W., Donini, O., Cieplak, P., Srinivasan, J., Case, D. A., and Cheatham, T. E. (2000) Calculating structures and free energies of complex molecules: Combining molecular mechanics and continuum models. *Acc. Chem. Res. 33*, 889–897.
36. Karplus, M., and Kushick, J. (1981) Method for estimating the configurational entropy of macromolecules. *Macromolecules 14*, 325–332.
37. Schlitter, J. (1993) Estimation of absolute and relative entropies of macromolecules using the covariance matrix. *Chem. Phys. Lett. 215*, 617–621.
38. Gil-Redondo, R., Estrada, J., Morreale, A., Herranz, F., Sancho, J., and Ortiz, A. R. (2009) VSDMIP: Virtual screening data management on an integrated platform. *J. Comput.-Aided Mol. Des. 23*, 171–184.
39. Ruiz, F. M., Gil-Redondo, R., Morreale, A., Ortiz, A. R., Fabrega, C., and Bravo, J. (2008) Structure-based discovery of novel non-nucleosidic DNA alkyltransferase inhibitors: Virtual screening and in vitro and in vivo activities. *J. Chem. Inf. Model. 48*, 844–854.
40. Kuntz, I. D., Blaney, J. M., Oatley, S. J., Langridge, R., and Ferrin, T. E. (1982) A geometric approach to macromolecule-ligand interactions. *J. Mol. Biol. 161*, 269–288.
41. Perez, C., and Ortiz, A. R. (2001) Evaluation of docking functions for protein-ligand docking. *J. Med. Chem. 44*, 3768–3785.
42. Lipinski, C. A., Lombardo, F., Dominy, B. W., and Feeney, P. J. (1997) Experimental and computational approaches to estimate solubility and permeability in drug discovery and development settings. *Adv. Drug Delivery Rev. 23*, 3–25.
43. Irwin, J. J., and Shoichet, B. K. (2005) ZINC—A free database of commercially available compounds for virtual screening. *J. Chem. Inf. Model. 45*, 177–182.
44. Wang, K., Murcia, M., Constans, P., Perez, C., and Ortiz, A. R. (2004) Gaussian mapping of chemical fragments in ligand binding sites. *J. Comput.-Aided Mol. Des. 18*, 101–118.
45. Huecas, S., and Andreu, J. M. (2004) Polymerization of nucleotide-free, GDP- and GTP-bound cell division protein FtsZ: GDP makes the difference. *FEBS Lett. 569*, 43–48.
46. Diaz, J. F., and Buey, R. M. (2007) Characterizing ligand-microtubule binding by competition methods. *Methods Mol. Med. 137*, 245–260.
47. Lakowicz, J. R. (1999) Principles of Fluorescence Spectroscopy, 2nd ed., Kluwer Academic/Plenum Publishers, New York.
48. Andreu, J. M., and Barasoain, I. (2001) The interaction of baccatin III with the taxol binding site of microtubules determined by a homogeneous assay with fluorescent taxoid. *Biochemistry 40*, 11975–11984.
49. Huecas, S., and Andreu, J. M. (2003) Energetics of the cooperative assembly of cell division protein FtsZ and the nucleotide hydrolysis switch. *J. Biol. Chem. 278*, 46146–46154.
50. Andreu, J. M., and Timasheff, S. N. (1982) Interaction of tubulin with single ring analogs of colchicine. *Biochemistry 21*, 534–543.
51. Fersht, A. R. (1987) The hydrogen-bond in molecular recognition. *Trends Biochem. Sci. 12*, 301–304.
52. Buey, R. M., Diaz, J. F., Andreu, J. M., O'Brate, A., Giannakakou, P., Nicolaou, K. C., Sasmal, P. K., Ritzen, A., and Namoto, K. (2004) Interaction of epothilone analogs with the paclitaxel binding site: Relationship between binding affinity, microtubule stabilization, and cytotoxicity. *Chem. Biol. 11*, 225–236.
53. Devoe, H., and Wasik, S. P. (1984) Aqueous solubilities and enthalpies of solution of adenine and guanine. *J. Solution Chem. 13*, 51–60.
54. Oliva, M. A., Trambaiolo, D., and Löwe, J. (2007) Structural insights into the conformational variability of FtsZ. *J. Mol. Biol. 373*, 1229–1242.

55. Jorgensen, W. L., and Duffy, E. M. (2002) Prediction of drug solubility from structure. *Adv. Drug Delivery Revs. 54*, 355–366.
56. Stokes, N. R., Sievers, J., Barker, S., Bennett, J. M., Brown, D. R., Collins, I., Errington, V. M., Foulger, D., Hall, M., Halsey, R., Johnson, H., Rose, V., Thomaides, H. B., Haydon, D. J., Czaplewski, L. G., and Errington, J. (2005) Novel inhibitors of bacterial cytokinesis identified by a cell-based antibiotic screening assay. *J. Biol. Chem. 280*, 39709–39715.
57. Plaza, A., Keffer, J. L., Bifulco, G., Lloyd, J. R., and Bewley, C. A. (2010) Chrysophaentins A-H, antibacterial bisdiarylbutene macrocycles that inhibit the bacterial cell division protein FtsZ. *J. Am. Chem. Soc. 132*, 9069–9077.
58. Hritz, J., Läppchen, T., and Oostenbrink, C. (2010) Calculations of binding affinity between C8-substituted GTP analogs and the bacterial cell-division protein FtsZ, *Eur. Biophys. J. 39*, 1573−1580.
59. Correia, J. J., Baty, L. T., and Williams, R. C. (1987) Mg^{2+} dependence of guanine-nucleotide binding to tubulin. *J. Biol. Chem. 262*, 17278–17284.
60. Kong, C. G., Ito, K., Walsh, M. A., Wada, M., Liu, Y. Y., Kumar, S., Barford, D., Nakamura, Y., and Song, H. W. (2004) Crystal structure and functional analysis of the eukaryotic class II release factor eRF3 from *S. pombe*. *Mol. Cell 14*, 233–245.
61. Sprang, S. R. (1997) G protein mechanisms: Insights from structural analysis. *Annu. Rev. Biochem. 66*, 639–678.